A Passive Broadband Impedance Equalizer for Improving the Input Return Loss of Electro-Absorption Modulators

Cheng Guan Lim, *Member, IEEE*

***Abstract*—Based on the context of an electro-absorption modulator integrated laser and the industry's standard 7-pin package having a RF connector, a complete module design that incorporates a simple yet effective broadband impedance equalizer to improve the input return loss of electro-absorption modulators (EAM) is proposed. The passive broadband impedance equalizer effectively reduces the input return loss of the EAM from between −9.84 and −5.26 dB to between −11.5 and −9.35 dB over a frequency range from 4.4 to 12.2 GHz without having to add a resistor in series with the EAM or reducing the EAM absorption-layer capacitance from the value that was optimized for optimal optical performance.**

***Index Terms*—Electro-absorption modulator (EAM), input return loss, impedance equalizer.**

I. Introduction

THE electro-absorption modulators (EAM) [1]–[12] have excellent extinction ratio and chirp performances compared to directly-modulated laser diodes [13], and offer a cheaper solution as well as lower operating voltage [14], [15] compared to lithium niobate Mach–Zehdner modulators (MZM) [16]–[18]. Hence, these devices are indeed very attractive to long-reach optical fiber communications networks. In a novel long-reach passive optical network architecture put forward recently as the next generation optical access networks, it was proposed to replace the wavelength-specific lasers in the customer transmitter with 10 Gb/s EAMs [19]. By doing so, this enables centralized optical carrier distribution and wavelength-independent modulation scheme to be employed, hence avoiding the inventory and deployment costs associated with the wavelength-specific lasers. Although the performances of EAMs are not quite comparable to that of the lithium niobate MZMs, their low operation voltage, small size, and the capability to be monolithically integrated with a distributed-feedback (DFB) laser to form an electro-absorption modulator integrated lasers (EML) [20]–[26] are the advantages of the EAMs over the lithium niobate MZMs. Without dispersion compensation, EMLs exhibiting a negative chirp and emitting at 1.55 μm can achieve 100 km [27] of transmission-span over standard single-mode optical fiber when operated at 10 Gb/s. When the above EMLs are operated at low extinction ratio, the transmission-span can be extended to 130 km [28]. Nevertheless, actual deployment limits the transmission-span of commercially available 10 Gb/s EML modules to 40 km [29]. When an amplifier is integrated with the EML, the resulting 10 Gb/s EML modules can achieve a transmission-span of 80 km [30]. Although semiconductors MZMs [31]–[34] that offer monolithic integration with a laser diode [35], [36] were developed to achieve the performances of the lithium niobate MZMs, their superb performances over EAMs and EMLs are limited to low bit-rates [37]. At higher bit-rates [38], [39], both EMLs and semiconductor MZMs have comparable performances. In addition, the monolithic integration of a semiconductor MZM with a laser diode is much more complicated and bulkier compared to EMLs.

Similar to laser diodes, EAMs have very low device resistance (typically around 5 Ω). Hence, impedance mismatch between the EAM and the signal source is a concern to these devices as this causes signal to be reflected back to the signal source resulting in degraded signal quality. To improve the input return loss (S_{11}) characteristics of EMLs, several techniques [40]–[42] have been proposed. However, these methods require a small resistance (typically a few ohms) to be added in series with the EAM section of the EML or the device capacitance of the EAM section of the EML be reduced from its optimized value in order to meet the RF specifications of EML modules. The disadvantages of adding a series resistor and reducing the device capacitance of the EAM section of EML are as follows.

1) The extinction ratio for a given signal magnitude is degraded due to loss of signal voltage developed across the series resistor.
2) The chirp performance may be compromised because changing the absorption-layer thickness alters the electric-field strength across the quantum-well (QW) absorption-layer and changes its band structure which may impose design constraints that prohibit the optimum chirp to be achieved.
3) The EAM is operated at a lower on-level optical output power in order to achieve a sizable on-off extinction ratio because on-off extinction ratio decreases with increasing input optical power and decreasing absorption strength (thicker absorption-layer leads to weaker electric-field strength across the absorption-layer and results in weaker absorption strength).

To alleviate the above problems while enabling the specifications for 10 Gb/s EML modules to be met, Lim has proposed

Manuscript received March 21, 2008; revised May 24, 2008. Current version published April 17, 2009.

The author was with the Department of Photonics/Institute of Electro-Optical Engineering, National Chiao Tung University, 1001 Ta Hsueh Road, Hsinchu 30010, Taiwan. He is now with the Network Photonics Research Center, National Institute of Advanced Industrial Science and Technology (AIST), Tsukuba, Ibaraki 305-8568, Japan (e-mail: c.g.lim@ieee.org).

Digital Object Identifier 10.1109/JLT.2008.2004969

0733-8724/$25.00 © 2009 IEEE

to use a lumped-element impedance-matching network (L-network) and to implement the L-network using distributed-element [43]. He has illustrated with a complete EML module design to show that the use of L-network enables the RF specifications for 10 Gb/s application to be met at less than half the device capacitance reduction from the typical optimized value as required by the other techniques. To reduce signal distortion due to input return loss/reflection without adding a series resistor or reducing the device capacitance of the EAM from its typical optimized value for 10 Gb/s applications, this paper illustrates with a complete EML module design (based on the industry's standard 7-pin package having a RF connector) that incorporates a simple yet effective broadband impedance equalizer to achieve an S_{11} of less than -10 dB for frequencies below 10 GHz or higher and a modulation bandwidth of at least 10 GHz (i.e., the RF specifications of 10 Gb/s EML modules). Without the series resistor, the signal voltage required to achieve any given on-off extinction ratio will be lower compared to the case where a resistor is inserted in series with the same EAM. Also, by not reducing the device capacitance of the EAM from the optimized value, the EAM can be operated with the optimum performance. As will be seen later, this is made possible by connecting a capacitive element at both ends of the signal-feeder [44] and bonding the EML onto a short-circuited stub. In the context of this work, the unique combination of the two capacitive elements and the short-circuited stub are referred to as the broadband impedance equalizer. In contrast to [42] where the characteristic impedance of the signal-feeder was uniformly reduced from 50 Ω to yield the appropriate reactive-trimming effect and [43] where the incorporation of the L-network causes the signal-feeder to exhibit a step-change in characteristic impedance at a particular point along the signal-feeder, connecting a capacitive element at both ends of the 50 Ω signal-feeder changes the characteristic impedance abruptly at both ends of the signal feeder. Nevertheless, that alone does not lead to the superior performance of the proposed EML module design. It is the unique combination of the two capacitive elements and the short-circuited stub that leads to EML module design with significantly improved performance.

II. Simulation Model and Approach

Fig. 1(a) shows the device structure of the EAM used in this study. The corresponding equivalent electrical circuit model of the EAM is shown in Fig. 1(b) where R1 represents the device resistance of the EAM, R2 the differential resistance of the EAM, C1 the capacitance of the absorption layer, C2 and C4 the intrinsic layers, C3 and C5 the iron-doped layers, C6 the polyimide layer. The value of these circuit elements for an EAM optimized to yield good optical performance for 10 Gb/s applications are 5 Ω, 300 Ω, 0.42, 0.732, 0.082, and 0.085 pF for R1, R2, C1, C2, and C4, C3 and C5, and C6, respectively.

Based on the industry's standard 7-pin package with a RF connector, a suitable equivalent electrical circuit model for simulating the S_{11} and modulation responses is shown in Fig. 2(a). In the event of deriving this equivalent electrical circuit model of the EML module, all factors have been evaluated for their influences on the RF performances of the EML module, and all insignificant factors have been excluded. The EAM is an electrical-optical device and its modulation bandwidth is limited by the device resistance and capacitance of the EAM. Thus, the modulation response of the EAM can be obtained in the simulation by connecting a termination resistor having a large value in parallel with the absorption-layer of the EAM. The configuration shown in Fig. 2(a) assumes no imperfection between the ground of the RF connector and the EML carrier. However, some finite ground imperfection between the RF connector and the EML carrier does exist in reality due to the bonding-wires that connect the ground planes of the above components. This ground imperfection can be taken into consideration in the simulation by using the data item component in the electrical circuit simulator of the Advanced Design System (ADS)—a well-established high-frequency simulation package developed by Agilent Technologies Corporation. Using the appropriate data item for a 2-port network, the S-parameters of the microstrip-line signal-feeder [represented by TL1 in Fig. 2(a)] on the EML carrier was simulated using ADS Momentum—a physical-layer electromagnetic simulator—and loaded into the electrical circuit simulation via the data item represented by SNP1 in Fig. 2(b). In this way, the ground imperfection between the RF connector and the EML carrier of the EML module can be taken into consideration by making an appropriate connection to the reference of the data item as illustrated in Fig. 2(b). In this equivalent electrical circuit model of the EML module, Term1 represents the 50 Ω characteristic impedance of the signal source, CPW1 the coplanar waveguide mounted on the 7-pin package where the signal lead of the RF connector (either a K-connector or GPO connector) is soldered, TL1 the signal-feeder on the EML carrier where the EML is bonded, R3 a thin-film resistor with a value of 50 Ω whose purpose is to increase the real part of the EML module input resistance to around 50 Ω, L1 the inductance of the bonding-wire connecting the signal line of CPW1 to the signal line of TL1, L2 the inductance of the bonding-wire connecting the ground of CPW1 to the ground of the EML

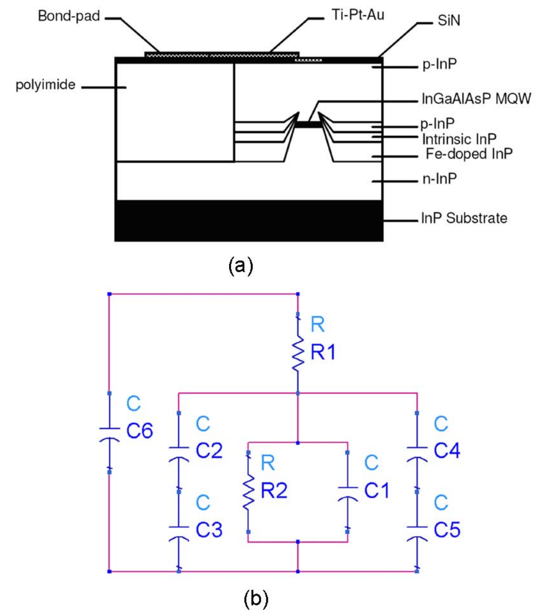

Fig. 1. (a) Device structure of the EAM and (b) the equivalent electrical circuit model of the EAM.

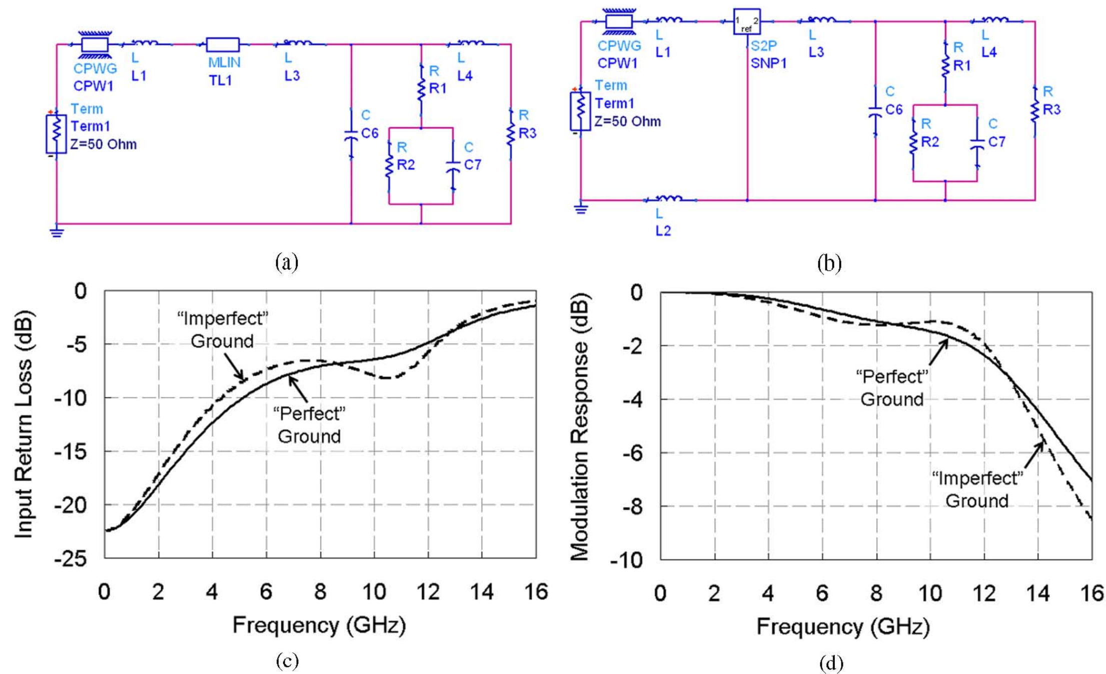

Fig. 2. Equivalent electrical circuit model of the EML module considering there is (a) no internal ground imperfection and (b) internal ground imperfection. (c) Input return loss responses and (d) modulation responses of the EML module design in (a) and (b).

carrier, L3 the inductance of the bonding-wire connecting the signal-feeder of TL1 to the bond-pad of the EAM section, L4 the inductance of the bonding-wire connecting the thin-film resistor R3 to the bond-pad of the EAM section, and C7 the total device capacitance of the EAM section.

In this work, a typical unit inductance of approximately 0.7 nH/mm was used for the bonding-wire. As a result, the values for L1, L2, L3, and L4 were 0.2 nH, 0.2 nH, 0.5 nH, and 0.5 nH, respectively. The length of TL1 was 3.4 mm and a high-frequency (HF) substrate with a thickness of 0.3 mm and a relative dielectric constant of 8.7 was used. Consequently, the width of the 50 Ω signal-feeder (i.e., TL1) is 0.323 mm. Based on all the above parameters, the S_{11} and modulation responses for the configurations shown in Fig. 2(a) and (b) were simulated and shown in Fig. 2(c) and (d), respectively. As can be observed, whether or not ground imperfection is considered does not cause a drastic difference in these responses. Simulation revealed that ground imperfection causes signal reflection to increase in general. However, due to the additional parasitic inductance introduced by the bonding-wire (L2) which effectively reduces some unfavorable capacitance of the EML module input impedance over the frequency range from approximately 7 GHz to 14 GHz, a dip appears on the S_{11} response. The reduction in capacitance of the EML module input impedance due to the parasitic inductance introduced by the bonding-wire (L2) is evident from the peaking of the modulation response starting at approximately 7 GHz and began to roll-off steeply at 12 GHz. Although ground imperfection causes the modulation response to decrease sharply for frequencies above 12 GHz, the 3 dB modulation bandwidth is essentially the same as that in the case with no ground imperfection. Though the effect of ground imperfection may not be really drastic and can be made negligible by using ribbon bonding-wires with extremely small inductance, ground imperfection has been taken into consideration in the following analysis in order to model the actual situation closely.

III. The Broadband Impedance Equalizer and Its Principle

As noted from Fig. 2(c), the S_{11} of the EML module rises above the −10 dB mark at 4.4 GHz. To reduce the S_{11} to less than −10 dB for frequencies of beyond 10 GHz in order to meet the specification for 10 Gb/s applications, it is proposed here to incorporate a unique broadband impedance equalizer on the EML carrier to dynamically control the input impedance of the EML module. The proposed unique broadband impedance equalizer consists of two capacitive elements and a short-circuited stub represented by C8, C9, and SNP2, respectively, in Fig. 3(a). To reduce the frequency-dependent signal distortion due to input reflection, two additional signal paths of which impedance is frequency-dependent were introduced. The purpose of introducing the above two additional signal paths is to provide a path for certain signal components, which would otherwise be reflected back to the signal source, to pass through. Since EAMs are voltage-operated and the above two signal paths are parallel to the EAM, the signal components flowing through C8 and C9 are not lost because the voltage of these signal components is still applied across the EAM. The idea of adding a capacitor at both end of a microstrip transmission-line to improve impedance-matching between two components of large contrasting impedance is not new. This technique had been demonstrated to improve the impedance-matching between a directly-modulated laser diode and a microwave signal source by Ghiasi *et al.* [44]. As will be seen in the following, the additional of a capacitor at either end of the microstrip transmission-line is not adequate to meet the S_{11}

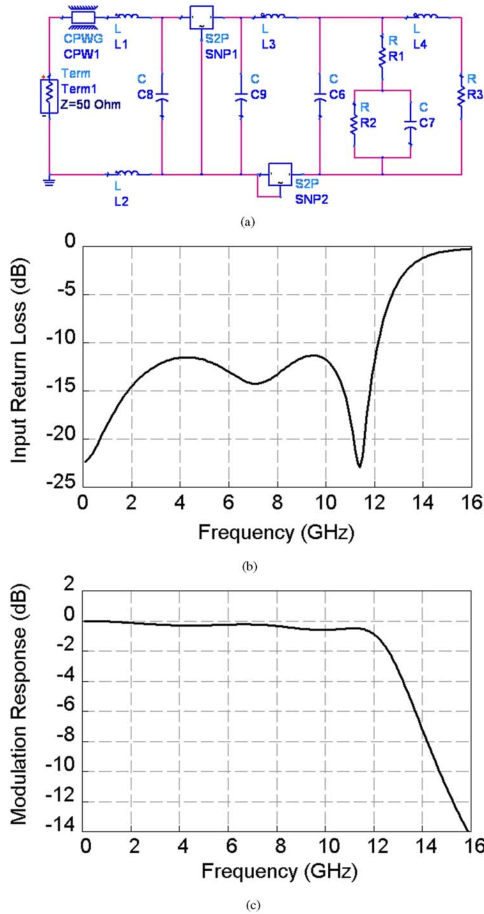

Fig. 3. (a) Equivalent electrical circuit model of the EML module with the proposed passive broadband impedance equalizer incorporated. (b) Nominal input return loss response and (c) nominal modulation response of the EML module design shown in Fig. 3(a).

requirement for 10 Gb/s EML modules. It will be shown in the following that a short-circuited stub [45] is necessary to extend the −10 dB cross-over frequency beyond 10 GHz below which the S_{11} is less than −10 dB.

IV. Performance Evaluation

The above broadband impedance equalizer was optimized to reduce the S_{11} to less than −10 dB for frequencies of up to beyond 10 GHz. As a result, the optimized nominal capacitance of C8 and C9 were found to be 0.26 pF and 0.46 pF respectively. The optimized length of the 50 Ω short-circuited stub was 0.5 mm. Using the nominal value for all the circuit elements of the equivalent circuit shown in Fig. 3(a), the S_{11} and modulation responses are shown in Fig. 3(b) and (c), respectively. As can be observed, the frequency range over which the S_{11} falls below −10 dB has improved significantly from 4.3 GHz to 12.1 GHz. The 3 dB modulation bandwidth was unchanged at approximately 13 GHz. Compared to the original design shown in Fig. 2(b), the incorporation of the passive broadband impedance equalizer has significantly reduced the S_{11} from between −9.84 dB and −5.26 dB to between −11.5 dB and −9.35 dB over the frequency range from 4.4 GHz to 12.2 GHz. The starting and ending values of the above frequency range

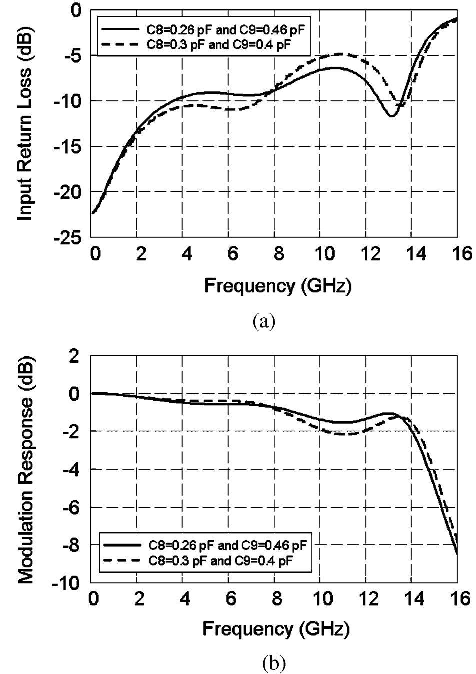

Fig. 4. (a) Input return loss response and (b) modulation response of the EML module design shown in Fig. 3(a) but with the short-circuited stub omitted.

correspond to the frequency at which the S_{11} of the original design and proposed design, respectively, rises above the −10 dB level.

The S_{11} characteristics and modulation responses for the case where the short-circuited stub was omitted are shown in Fig. 4(a) and (b), respectively. As can be observed, the S_{11} rose above −10 dB at 3.5 GHz. The −10 dB cross-over frequency can be extended to slightly more than 7 GHz by re-optimizing the value of C8 and C9 to achieve the best S_{11} response in the above case. Compared to the case in Fig. 3(c), the case where the short-circuited stub was omitted shows a wider modulation bandwidth; the former has a modulation bandwidth of approximately 13 GHz whereas the latter has a modulation bandwidth of nearly 15 GHz. Nevertheless, the latter exhibits a more severe slump on the modulation response over a frequency range from 8 GHz to 12 GHz.

V. Design Implementation

The best implementation of the EML module design shown in Fig. 3(a) would probably be the one that does not introduce additional component-count and complication compared to the original design shown in Fig. 2(b). Therefore, the best approach is to implement the capacitors (i.e., C8 and C9) of the broadband impedance equalizer on the HF substrate of the EML carrier. Here, the microstrip transmission-line has been chosen as a mean of illustration. Since the short-circuited stub has a length of 0.5 mm and width of 0.323 mm and the length of EMLs for 10 Gb/s applications is typically within the range from 450 μm to 500 μm, it would certainly be ideal to use it as the bond-pad of the EML too.

Based on the dielectric constant and thickness of the HF substrate used, the required dimensions to obtain the optimum value of C8 and C9 were calculated. Many combinations of length

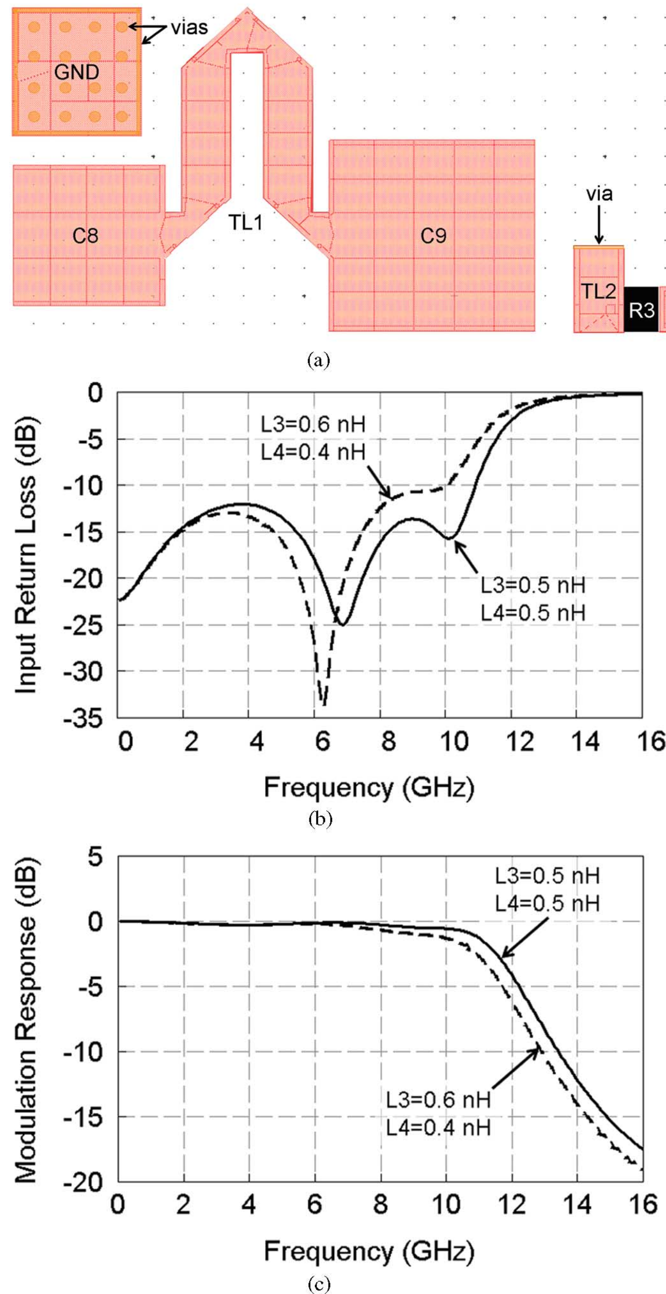

Fig. 5. (a) One of the possible EML carrier designs that incorporates the passive broadband impedance equalizer. (b) Input return loss response and (c) modulation response of the EML module having the EML carrier design shown in Fig. 5(a).

and width are possible to achieve the designed value of C8 and C9, however the feasibility of these combinations depend on the space constraint of the 7-pin package. For illustration purpose, the shape of the microstrip transmission-lines that represent C8 and C9 were chosen to be square. With all the above considerations in mind, one possible design of the EML carrier is shown in Fig. 5(a). It is worth mentioning that the isolation resistance between the EAM and the DFB laser of the EML is typically 20 kΩ or larger. Hence, the d.c. biasing portion for the DFB laser does not affect the HF performance of the EML and has not been included in the EML carrier design shown in Fig. 5(a) since it is not essential to the scope of this work.

The self-explanatory artwork shown in Fig. 5(a) was constructed using the layout editor of ADS Momentum simulator. The patches that represent C8 and C9 have a side dimension of 1.006 and 1.367 mm, respectively. The length of TL1 was the same as that of the original design (i.e., 3.4 mm) so that a direct comparison with the original design can be made to make the study of the mechanism of the broadband impedance equalizer easier. One end of TL2 is connected to the ground plane on the under-side of the HF substrate via edge via and this microstrip transmission-line represents the short-circuited stub as well as the bond-pad for the EML.

VI. Performance and Tolerance Evaluation of Design Implementation

With the design implementation shown in Fig. 5(a), the S_{11} and modulation responses were simulated by importing the S-parameters of the design implementation as produced by the ADS Momentum simulator into the ADS circuit simulator. The ADS Momentum simulator is a powerful electromagnetic simulator that simulates the electromagnetic characteristics of an actual design implementation closely. Consequently, compared to the nominal S_{11} response of this design in equivalent electrical circuit form [Fig. 3(b)], the nominal S_{11} response [Fig. 5(b)] of the above design implementation exhibits a relatively narrower frequency range over which the S_{11} is less than -10 dB. In equivalent electrical circuit form, the design exhibits a cross-over frequency of 12.2 GHz below which the S_{11} is less than -10 dB. In the case of the above design implementation, the cross-over frequency is reduced to 11 GHz. The reduction in cross-over frequency in the latter case is attributed mainly to the parasitic inductances introduced by the implementation of C8 and C9 shown in Fig. 5(a). Correspondingly, the nominal modulation bandwidth of the design implementation [Fig. 5(c)] is reduced from approximately 13 GHz to 11.8 GHz.

Generally, the value of L1 and L2 is typically of about 0.1 nH and will not exceed 0.2 nH. Hence, some performance margin has already been incorporated by assuming the value of L1 and L2 to be 0.2 nH. As for microstrip transmission-line fabcrication, very high precision can be achieved through calibrations. Hence, any possible deviations of the dimensions from the design values are expected to be small enough to allow any possible resulting differences in the performance of the EML modules to be neglected. Having considered the above factors, the S_{11} and modulation responses of the design implementation were evaluated to determine the tolerance of L3 and L4. As will be seen in the following, evaluation shows that the upper limit of the value of L3 and the lower limit of L4 are limited by the cross-over frequency and this corresponds to the first-occurring worst-case of the design implementation. The value of L3 should not be less than 0.31 nH and L4 should not have an inductance greater than 0.68 nH, otherwise the peak of the S_{11} response at 4.5 GHz and 9.6 GHz, respectively, will rise above -10 dB. In either case, the modulation bandwidth was noted to be in excess of 10 GHz. The modulation response for the case where the value of L3 and L4 are 0.6 nH and 0.4 nH, respectively, is shown in Fig. 5(b). As is evident from the above, this case represents the first-occurring worst-case of this design implementation and limits the tolerance of L3 and L4 to ± 0.1 nH.

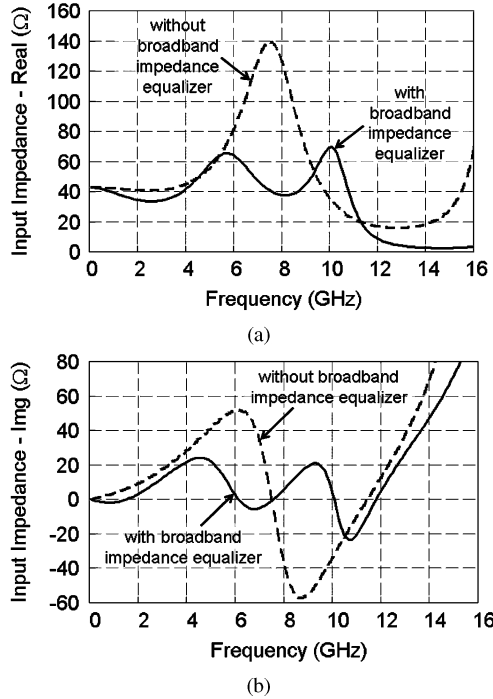

Fig. 6. (a) Real part and (b) imaginary part of the input impedance of the original EML module design shown in Fig. 2(b) and the proposed EML module design shown in Fig. 3(a) considering the EML carrier design shown in Fig. 5(a).

VII. Mechanism of the Broadband Impedance Equalizer

In Section III, the principle of the broadband impedance equalizer was briefly explained in the context of signal flow. As that is a very general explanation, a detailed illustration of the mechanism of the broadband impedance equalizer based on the input impedance $(Z_{\rm in})$ of the EML module will be presented in this section.

The real and imaginary parts of $Z_{\rm in}$ for the original design [Fig. 2(b)] and the proposed design [Fig. 3(a) with the EML carrier design presented in Fig. 5(a)] are shown in Fig. 6(a) and (b), respectively. As can be observed, the real part of $\mathrm{Z_{in}}(\mathrm{Re}\{Z_{\rm in}\})$ for the original design stays at approximately 40 Ω for frequencies below 4 GHz, but rises rapidly thereafter to nearly 140 Ω at 7.5 GHz before falling rapidly to approximately 20 Ω over the frequency range from 11 GHz to 14.5 GHz. Beyond 14.5 GHz, $\mathrm{Re}\{Z_{\rm in}\}$ starts to rise rapidly again. From the response of the imaginary part of $Z_{\rm in}(\mathrm{Im}\{Z_{\rm in}\})$, it was noted that $Z_{\rm in}$ is inductive for frequencies below approximately 6 GHz, and $\mathrm{Im}\{Z_{\rm in}\}$ increases gradually with increasing frequency to $j52\ \Omega$. Over the frequency range from approximately 6 GHz to nearly 9 GHz, $Z_{\rm in}$ falls sharply and becomes capacitive at 7.5 GHz. For frequencies above 8.7 GHz, $\mathrm{Im}\{Z_{\rm in}\}$ increases gradually from nearly $-j60\ \Omega$ at 8.7 GHz. Above 11.4 GHz, $Z_{\rm in}$ becomes inductive. The above large variation in $Z_{\rm in}$ is the result of poor impedance matching between the EML module and the HF signal source. Consequently, the $\mathrm{S_{11}}$ of the EML module is poor.

With the incorporation of the broadband impedance equalizer in the proposed design, the magnitudes of the variation of $\mathrm{Re}\{Z_{\rm in}\}$ and $\mathrm{Im}\{Z_{\rm in}\}$ are significantly reduced. For frequencies below 11 GHz, the variation of $\mathrm{Re}\{Z_{\rm in}\}$ has been controlled to within 30 Ω to 70 Ω. Over a frequency range from 10 GHz to 12 GHz, $\mathrm{Re}\{Z_{\rm in}\}$ decreases sharply from nearly 70 Ω to nearly 9 Ω, and has an average value of approximately 3 Ω thereafter. The latter phenomenon is the result of C8 crippling the effect of R3. The two peaks observed on the response of $\mathrm{Re}\{Z_{\rm in}\}$ is the result of C8 and C9 whose purpose is to control the variation of $\mathrm{Im}\{Z_{\rm in}\}$. The input impedance of the EML modules for the proposed design is slightly capacitive for frequencies below approximately 1.5 GHz. Thereafter, $\mathrm{Im}\{Z_{\rm in}\}$ increases gradually with increasing frequency as in the original design. However, due to the effect of C9, $\mathrm{Im}\{Z_{\rm in}\}$ starts to decrease gradually at approximately 4.5 GHz and become capacitive at slightly above 6 GHz. Due to the short-circuited stub (i.e., TL2), $\mathrm{Im}\{Z_{\rm in}\}$ starts to increase gradually at a frequency of nearly 7 GHz. To prevent $\mathrm{Im}\{Z_{\rm in}\}$ from decreasing to the values that cause the $\mathrm{S_{11}}$ to become greater than -10 dB as observed in Fig. 4(a), the short-circuited stub was optimized to increase $\mathrm{Im}\{Z_{\rm in}\}$ gradually over the frequency range from nearly 7 GHz to slightly above 9 GHz. As a result, $\mathrm{Im}\{Z_{\rm in}\}$ was increased from $-j5.7\ \Omega$ to $j21\ \Omega$ over the frequency range as stated in the above. Thereafter, C8 causes $\mathrm{Im}\{Z_{\rm in}\}$ to decrease rapidly to $-j23\ \Omega$ at approximately 11 GHz. Beyond that, $\mathrm{Im}\{Z_{\rm in}\}$ increases as in the original design. As a whole, the proposed broadband impedance equalizer enables $\mathrm{Re}\{Z_{\rm in}\}$ and $\mathrm{Im}\{Z_{\rm in}\}$ to be well-controlled to within $50 \pm 20\ \Omega$ and $\pm j25\ \Omega$, respectively, which would otherwise vary from 22 Ω to 139 Ω and $j52\ \Omega$ to $-j57\ \Omega$, respectively, for frequencies below 11 GHz. Consequently, the $\mathrm{S_{11}}$ of the proposed EML module design was kept under -10 dB for frequencies below 11 GHz.

VIII. Conclusion

Without resorting to the addition of a series resistor and reduction of the EAM device capacitance from its optimum value for 10 Gb/s applications, a simple yet effective technique has been proposed and demonstrated to greatly reduce the input return loss of EAM/EML modules. Over a frequency range from 4.4 GHz to 12.2 GHz, the input return loss has been reduced to between -11.5 dB and -9.35 dB from between -9.84 dB and -5.26 dB. This is the result of improved impedance matching between the EAM and the signal source brought about by the passive broadband impedance equalizer proposed in this work. The passive broadband impedance equalizer consisted of the unique combination of two capacitive elements connected at the ends of the conventional signal feeder and a short-circuited stub onto which the EAM was bonded. The two capacitive elements created two paths for certain signal components to pass through instead of reflected back to the signal source, and the short-circuited stub trimmed off excessive unfavorable reactances over a small range of frequencies. Thus, the passive broadband impedance equalizer has a three-degree of freedom which enabled it to out-perform other impedance matching techniques reported for EAMs/EMLs. The passive broadband impedance equalizer can be easily implemented using distributed elements such as the microstrip lines. Hence, it can be easily incorporated on the EAM/EML carrier. Reduced input return loss using no additional component and no series

TABLE I
PARAMETERS USED IN THE SIMULATIONS

Parameter	Symbol	Value
Device resistance of EAM	R1	5 Ω
Differential resistance of EAM	R2	300 Ω
Thin-film resistor	R3	50 Ω
Capacitance of EAM absorption layer	C1	0.42 pF
Capacitance of EAM intrinsic layers	C2, C4	0.732 pF
Capacitance of EAM iron-doped layers	C3, C5	0.082 pF
Capacitance of EAM polyimide layers	C6	0.085 pF
Equivalent capacitance of C1,C2,C3,C4,C5,C6	C7	0.579 pF
Capacitance of impedance equalizer	C8	0.26 pF
Capacitance of impedance equalizer	C9	0.46 pF
Bonding-wires	L1, L2	0.2 nH
Bonding-wires	L3, L4	0.5 nH
Characteristic impedance of microwave systems	Term1	50 Ω
Relative dielectric constant of CPW1	-	9.5
Length of signal and ground planes of CPW1	-	0.67 mm
Width of signal plane of CPW1	-	0.3 mm
Gap between signal and ground planes of CPW1	-	0.24 mm
Substrate thickness of CPW1	-	0.38 mm
Relative dielectric constant of TL1	-	8.7
Length of signal plane of TL1	-	3.4 mm
Width of signal plane of TL1	-	0.323 mm
Substrate thickness of TL1	-	0.3 mm
Length of signal plane of TL2	-	0.5 mm
Width of signal plane of TL2	-	0.323 mm
Substrate thickness of TL2	-	0.3 mm

resistor or reduction of the EAM device capacitance means EAM/EML modules with enhanced performances and lower power consumption.

APPENDIX

The information on all the circuit elements used in the simulations is shown in Table I.

ACKNOWLEDGMENT

The author would like to thank the Chips Implementation Center (C.I.C.) for the loan of the Advanced Design System—a popular and well-established commercial HF computer-aided-design package.

REFERENCES

[1] K. Wakita, Y. Kawamura, Y. Yoshinkuni, and H. Asahi, "Longwavelength waveguide multi-quantum-well (MQW) optical modulator with 30:1 on/off ratio," *Electron. Lett.*, vol. 22, pp. 907–908, Aug. 1986.

[2] T. Kataoka, Y. Miyamoto, K. Hagimoto, K. Wakita, and I. Kotaka, "Ultrahigh-speed driverless MQW intensity modulator, and 20 Gbit/s 100 km transmission experiments," *Electron. Lett.*, vol. 28, pp. 897–898, May 1992.

[3] O. Mitomi, I. Kotaka, K. Wakita, S. Nojima, K. Kawano, Y. Kawamura, and H. Asai, "40-GHz bandwidth InGaAs/InAlAs multiple quantum well optical intensity modulator," *Appl. Opt.*, vol. 31, pp. 2030–2035, Apr. 1992.

[4] H. Arimoto, J. Shimizu, M. Shirai, and M. Aoki, "Wide temperature range, from 0 to 85°C, operation of a 1.55 μm, 40 Gbit/s InGaAlAs electro-absorption optical modulator," *Electron. Lett.*, vol. 41, pp. 764–766, Jan. 2005.

[5] T. Okiyama, H. Nishimoto, I. Yokota, and T. Touge, "Evaluation of 4-Gbit/s optical fiber transmission distance with direct and external modulation," *IEEE J. Lightw. Technol.*, vol. 6, no. 11, pp. 1686–1692, Nov. 1988.

[6] K. Wakita, I. Kotaka, O. Mitomi, H. Asai, and Y. Kawamura, "Observation of low-chirp modulation in InGaAs-InAlAs multiple-quantum-well optical modulators under 30 GHz," *IEEE Photon. Technol. Lett.*, vol. 3, no. 2, pp. 138–140, Feb. 1991.

[7] O. Mitomi, S. Nojima, I. Kotaka, K. Wakita, K. Kawano, and M. Naganuma, "Chirping characteristic and frequency response of MQW optical intensity modulator," *J. Lightw. Technol.*, vol. 6, no. 1, pp. 71–77, Jan. 1992.

[8] J. Langanay, C. Stark, M. Boulou, M. Nicolardot, J. Y. Emery, C. Fortin, P. Aubert, and D. Lesterlin, "Low spectral chirp and large electroabsorption in a strained InGaAsP/InGaAsP multiple quantum well modulator," *Appl. Phys. Lett.*, vol. 62, pp. 2066–2068, Apr. 1993.

[9] F. Devaux, A. Ougazzaden, A. Mircea, A. Ramdane, P. Krausz, J. Semo, F. Huet, M. Carré, and A. Carenco, "Zero-loss multiple-quantum-well electroabsorption modulator with very low chirp," *Appl. Phys. Lett.*, vol. 64, pp. 954–956, Feb. 1994.

[10] F. Dorgeuille and F. Devaux, "On the transmission performances and the chirp parameter of a multiple-quantum-well electroabsorption modulator," *IEEE J. Quantum Electron.*, vol. 30, pp. 2565–2572, Nov. 1994.

[11] N. Suzuki and Y. Hirayama, "Comparison of effective α parameters for multiquantum-well electroabsorption modulators," *IEEE Photon. Technol. Lett.*, vol. 7, no. 9, pp. 1007–1009, Sep. 1995.

[12] K. Wakita, K. Yoshino, I. Kotaka, S. Kondo, and Y. Noguchi, "Blue-chirp electroabsorption modulators with very thick quantum wells," *IEEE Photon. Technol. Lett.*, vol. 8, no. 9, pp. 1169–1171, Sep. 1996.

[13] K. Sato, S. Kuwahara, and Y. Miyamoto, "Chirp characteristics of 40-Gb/s directly modulated distributed-feedback laser diodes," *J. Lightw. Technol.*, vol. 23, no. 11, pp. 3790–3797, Nov. 2005.

[14] F. Devaux, F. Dorgeuille, A. Ougazzaden, F. Huet, M. Carré, A. Carenco, M. Henry, Y. Sorel, J. F. Kerdiles, and E. Jeanney, "20 Gbit/s operation of high-efficiency InGaAsP/InGaAsP MQW electroabsorption modulator with 1.2 V drive voltage," *IEEE Photon. Technol. Lett.*, vol. 5, no. 11, pp. 1288–1290, Nov. 1993.

[15] T. Ido, H. Sano, D. J. Moss, S. Tanaka, and A. Takai, "Strained InGaAs/InAlAs MQW electroabsorption modulators with large bandwidth and low driving voltage," *IEEE Photon. Technol. Lett.*, vol. 6, no. 11, pp. 1207–1209, Oct. 1994.

[16] K. Kawano, T. Kitoh, H. Jumonji, T. Nozawa, and M. Yanagibashi, "New traveling-wave electrode Mach–Zehnder optical modulator with 20 GHz bandwidth and 4.7 V driving voltage at 1.52 μm wavelength," *Electron. Lett.*, vol. 25, pp. 1382–1383, Sep. 1989.

[17] K. Noguchi, H. Miyazawa, and O. Mitomi, "75 GHz Ti:$LiNbO_3$ optical modulator with ridge structure," *Electron. Lett.*, vol. 30, pp. 949–950, Jun. 1994.

[18] K. Noguchi, H. Miyazawa, and O. Mitomi, "Frequency-dependent propagation characteristics of coplanar waveguide electrode on 100 GHz Ti:$LiNbO_3$ optical modulator," *Electron. Lett.*, vol. 34, pp. 661–663, Apr. 1998.

[19] G. Talli and P. D. Townsend, "Hybrid DWDM-TDM long-reach PON for next-generation optical access," *J. Lightwave Technol.*, vol. 24, no. 7, pp. 2827–2834, Jul. 2006.

[20] M. Suzuki, Y. Noda, H. Tanaka, S. Akiba, Y. Kushiro, and H. Isshiki, "Monolithic integration of InGaAsP/InP distributed feedback laser and electroabsorption modulator by vapor phase epitaxy," *J. Lightwave Technol.*, vol. 5, no. 9, pp. 1277–1285, Sep. 1987.

[21] M. Aoki, H. Sano, M. Suzuki, M. Takahashi, K. Uomi, and A. Takai, "Novel structure MQW electroabsorption-modulator/DFB-laser integrated device fabricated by selective area MOCVD growth," *Electron. Lett.*, vol. 27, pp. 2138–2140, Nov. 1991.

[22] M. Aoki, M. Takahashi, M. Suzuki, H. Sano, K. Uomi, T. Kawano, and A. Takai, "High-extinction-ratio MQW electroabsorption-modulator integrated DFB laser fabricated by in-plane bandgap energy control technique," *IEEE Photon. Technol. Lett.*, vol. 4, no. 6, pp. 580–582, Jun. 1992.

[23] I. Kotaka, K. Wakita, M. Okamoto, H. Asai, and Y. Kondo, "A low-drive-voltage, high-speed monolithic multiple-quantum-well modulator/DFB laser light source," *IEEE Photon. Technol. Lett.*, vol. 5, no. 1, pp. 61–63, Jan. 1993.

[24] M. Aoki, M. Suzuki, H. Sano, T. Kawano, T. Ido, T. Taniwatari, K. Uomi, and A. Takai, "InGaAs/InGaAsP MQW electro-absorption modulator integrated with a DFB laser fabricated by bandgap energy control selective area MOCVD," *IEEE J. Quantum Electron.*, vol. 29, no. 6, pp. 2088–2096, Jun. 1993.

[25] K. Morito, R. Sahara, K. Sato, Y. Kotaki, and H. Soda, "High power modulator integrated DFB laser incorporating strain-compensated MQW and graded SCH modulator for 10 Gbit/s transmission," *Electron. Lett.*, vol. 31, pp. 975–976, Jun. 1995.

[26] Y. Miyazaki, H. Tada, T. Aoyagi, T. Nishimura, and Y. Mitsui, "Extremely small-chirp electroabsorption-modulator integrated distributed feedback laser diode with a shallow quantum-well absorption layer," *IEEE J. Quantum. Electron.*, vol. 38, no. 8, pp. 1075–1080, Aug. 2002.

[27] K. Morito, R. Sahara, K. Sato, and Y. Kotaki, "Penalty-free 10 Gb/s NRZ transmission over 100 km of standard fiber at 1.55/spl mu/m with a blue-chirp modulator integrated DFB laser," *IEEE Photon. Technol. Lett.*, vol. 8, no. 3, pp. 431–433, Mar. 1996.

[28] Y. K. Park, T. V. Nguyen, P. A. Morton, J. E. Johnson, O. Mizuhara, J. Jeong, L. D. Tzeng, P. D. Yeates, T. Fullowan, P. F. Sciortino, A. M. Sergent, W. T. Tsang, and R. D. Yadvish, "Dispersion-penalty-free transmission over 130-km standard fiber using a 1.55-/spl mu/m, 10-Gb/s integrated EA/DFB laser with low-extinction ratio and negative chirp," *IEEE Photon. Technol. Lett.*, vol. 8, pp. 1255–1257, Sep. 1996.

[29] Y. D. Bae, B. K. Kang, B. Park, S. M. Lee, Y. H. Kim, H. K. Kim, M. K. Park, I. Kim, and D. H. Jang, "Operation of 1550-nm electroabsorption-Modulated laser at 40°C for 10-Gb/s, 40-km transmission," *IEEE J. Sel. Topics Quantum Electron.*, vol. 11, no. 1, pp. 135–140, Jan.–Feb. 2005.

[30] I. Kim, B. K. Kang, Y. D. Bae, B. Park, S. M. Lee, Y. H. Kim, and D. H. Jang, "Design of amplifier- and modulator-integrated laser diode for 10-Gb/s 80-km transmission," *IEEE J. Sel. Topics Quantum Electron.*, vol. 11, no. 2, pp. 323–328, Mar.–Apr. 2005.

[31] C. Rolland, R. S. Moore, F. R. Shepherd, and G. Hillier, "10 Gbit/s 1.56 μm multiquantum well InP/InGaAsP Mach–Zehnder optical modulator," *Electron. Lett.*, vol. 29, pp. 471–472, Mar. 1993.

[32] J. Yu, C. Rolland, D. Yevick, A. Somani, and S. Bradshaw, "Phase-engineered III-V MQW Mach–Zehnder modulators," *IEEE Photon. Technol. Lett.*, vol. 8, no. 8, pp. 1018–1020, Aug. 1996.

[33] C. Lawetz, J. C. Cartledge, C. Rolland, and J. Yu, "Modulation characteristics of semiconductor Mach–Zehnder optical modulators," *J. Lightwave Technol.*, vol. 15, no. 4, pp. 697–703, Apr. 1997.

[34] S. Akiyama, H. Itoh, T. Takeuchi, A. Kuramata, and T. Yamamoto, "Low-chirp 10 Gbit/s InP-based Mach–Zehnder modulator driven by 1.2 V single electrical signal," *Electron. Lett.*, vol. 41, pp. 40–41, Jan. 2005.

[35] J. E. Zucker, K. L. Jones, M. A. Newkirk, R. P. Gnall, B. I. Miller, M. G. Young, U. Koren, C. A. Burrus, and B. Tell, "Quantum well interferometric modulator monolithically integrated with 1.55 μm tunable distributed Bragg reflector laser," *Electron. Lett.*, vol. 28, pp. 1888–1889, Sep. 1992.

[36] T. Tanbun-Ek, P. F. Sciortino, Jr., A. M. Sergent, K. W. Wecht, P. Wisk, Y. K. Chen, C. G. Bethea, and S. K. Sputz, "DFB lasers integrated with Mach–Zehnder optical modulator fabricated by selective area growth MOVPE technique," *IEEE Photon. Technol. Lett.*, vol. 7, no. 9, pp. 1019–1021, Sep. 1995.

[37] D. M. Adams, C. Rolland, A. Fekecs, D. McGhan, A. Somani, S. Bradshaw, M. Poirier, E. Dupont, E. Cremer, and K. Anderson, "1.55 μm transmission at 2.5 Gbit/s over 1102 km of NDSF using discrete and monolithically integrated InGaAsP/InP Mach–Zehnder modulator and DFB laser," *Electron. Lett.*, vol. 34, pp. 771–773, Apr. 1998.

[38] P. Delansay, D. Penninckx, S. Artigaud, J.-G. Provost, J.-P. Hebert, E. Boucherez, J. Y. Emery, C. Fortin, and O. Le Gouezigou, "10 Gbit/s transmission over 90–127 km in the wavelength range 1530–1560 nm using an InP-based Mach–Zehnder modulator," *Electron. Lett.*, vol. 32, pp. 1820–1821, Sep. 1996.

[39] D. M. Adams, C. Rolland, N. Puetz, R. S. Moore, F. R. Shepherd, H. B. Kim, and S. Bradshaw, "Mach-Zehnder modulator integrated with a gain-coupled DFB laser for 10 Gbit/s, 100 km NDSF transmission," *Electron. Lett.*, vol. 32, pp. 485–487, Feb. 1996.

[40] E. Ishimura, Y. Miyazaki, and M. Kawano, "Light Modulator Module and Method for Fabricating Light Modulator Module," U.S. Patent 5 602 672, Feb. 11, 1997.

[41] S. H. Lee, J. H. Ahn, Y. K. Oh, J. S. Ma, A. G. Choo, T. I. Kim;, Y. Kim, and J. Jeong, "High performance modules of 2.5 Gbps modulator integrated DFB lasers using new RF impedance matching technique," *IEEE Trans. Adv. Packag.*, vol. 24, no. 3, pp. 407–410, Aug. 2001.

[42] C. G. Lim, "The effect of signal-feeder characteristic impedance on the signal injection efficiency of electro-absorption modulator integrated lasers," *J. Lightw. Technol.*, vol. 24, no. 10, pp. 3835–3841, Oct. 2006.

[43] C. G. Lim, "Electro-absorption modulator integrated lasers with enhanced signal injection efficiency," *J. Lightw. Technol.*, vol. 26, pp. 685–691, Mar. 2008.

[44] A. Ghiasi and A. Gopinath, "Novel wide-bandwidth matching technique for laser diodes," *IEEE Trans. Microw. Theory Technol.*, vol. 38, no. 5, pp. 673–675, May 1990.

[45] D. M. Pozar, *Microwave Engineering*. Hoboken, NJ: Wiley, 2000.

Cheng Guan Lim (S'94–M'00) received the B.Eng. (hons.) degree in electronic and electrical engineering and the Ph.D. degree at the Institute of Microwaves and Photonics of the School of Electronic and Electrical Engineering from the University of Leeds, Leeds, U.K., in 1997 and 2001, respectively.

From 2001 to 2003, he was a Research Engineer at the Yokohama Research and Development Laboratories, The Furukawa Electric Company, Yokohama, Japan, working on the development of semiconductor laser modules for digital and analog telecommunication applications. In 2003, he joined Agilent Technologies, Singapore, as a Senior Engineer focusing on optoelectronic device manufacturing. From 2004 to 2005, he was a Senior Research Scientist at the Institute for Infocomm Research-Singapore (a member of the Agency for Science, Technology and Research-Singapore, and a National University of Singapore affiliated research institute) dealing with radio-over-fiber technologies. He was an Assistant Professor at the Department of Photonics/Institute of Electro-Optical Engineering, National Chiao Tung University, Hsinchu, Taiwan. Currently, he is a Researcher at the National Institute of Advanced Industrial Science and Technology, Tsukuba, Japan, where he conducts research on intersubband transitions in InGaAs–AlAs–AlGaAsSb coupled double-quantum-wells. His prime research interests include the investigation of the fundamental physics of advanced nanostructures and the optical and electronic properties of advanced novel materials through simulation and experimentation. His secondary research interests are photonic packaging, RF photonics, and photonic integrated circuits. He has one granted U.S. patent, written one invention disclosure, and published several international refereed journal and conference papers.

Dr. Lim has served as a Steering Committee Member for the Inaugural IEEE International Workshop on Antenna Technology 2005 (Singapore), and as a Technical Program Committee member for the 2005 Symposium on Technology Fusion of Optoelectronics and Communications-International Conference on Photonics, Taiwan. In 1995, he was awarded the Crab Tree Prize for outstanding academic achievement, the Hewlett-Packard Prize in 1997 for the recognition as the best student in High-Frequency Engineering, and the F. W. Carter Prize in 2001 for presenting the best Ph.D. dissertation.